Hindawi
Advances in Civil Engineering
Volume 2021, Article ID 5549147, 12 pages
https://doi.org/10.1155/2021/5549147

Research Article

Effects of Cyclic Loading on the Pore Structure of Anthracite Coal

Dong Wang,[1,2,3] Tie Li,[1] Zhiheng Cheng,[4] and Weihua Wang[2,3]

[1]*State Key Laboratory of High-Efficiency Mining and Safety of Metal Mines, Ministry of Education, School of Civil and Resource Engineering, University of Science and Technology Beijing, Beijing 100083, China*
[2]*China Coal Research Institute, Beijing 100013, China*
[3]*State Key Laboratory of Coal Mining and Clean Utilization (China Coal Research Institute), Beijing 100013, China*
[4]*School of Safety Engineering, North China Institute of Science and Technology, Beijing 101601, China*

Correspondence should be addressed to Zhiheng Cheng; an958158@163.com

Received 15 February 2021; Revised 11 April 2021; Accepted 17 April 2021; Published 29 April 2021

Academic Editor: Gong-Da Wang

In the process of improving coalbed permeability through pulse hydraulic fracturing, the cyclic loading effect influences the characteristics of micropores in coal matrix, thus affecting the process of gas migration. Therefore, it is essential to investigate the effect of cyclic loading on the pore structure of coal. Seven groups of loading tests at different frequencies and amplitudes were conducted on anthracite coal obtained from Shanxi Province, China, using a fatigue-testing machine. Subsequently, using a PoreMaster GT-60 Mercury-intrusion apparatus, the influence of the frequency and amplitude on the structural characteristics (including mercury-injection and mercury-ejection curves, pore size distribution, porosity, and specific surface area) of pores in coal samples was analyzed. Finally, the law and mechanism of action of the loading frequency and amplitude on pores in coal samples were comprehensively analyzed. The test results showed that, in the case of maintaining the sine-wave amplitude unchanged during loading while altering the loading frequency, the overall porosity and pore volume rise at different degrees. The growth of the loading frequency presents a more significant promotive effect on the initiation and development of pores and fractures. Moreover, it drives the transformation of micropores and transition pores into mesopores and macropores, thus increasing the proportion of seepage pores. Under the condition of large sine-wave amplitude during loading, macropores and mesopores are subjected to the repeated action of the external force, thereby reducing the overall porosity. In addition, the volume of the seepage pores declines, and the number of the coalesced pores decreases. Finally, in light of these results, the implications of frequency and amplitude selection in the process of pulse hydraulic fracturing are discussed. Therefore, the results of this research will provide an important theoretical basis for the field application of pulse hydraulic fracturing technology in coal mines.

1. Introduction

Efficient extraction of coalbed methane (CBM) is important for the safe production of coal in many underground coal mines [1, 2]. Additionally, the extracted CBM can be used as energy, and the combustion of CBM can be part of the environmental protection plan of coal mine enterprises, because it can avoid the release of the greenhouse gas (CH_4) into the atmosphere [3–5]. However, the permeability of coal seams in China is generally low, which is unfavorable for the production and utilization of CBM [6, 7]. At present, hydraulic fracturing has been widely used to improve the yield of CBM reservoirs [8–10]. The technology can enhance the permeability of coal seams by increasing the number and density of fractures, thus changing the structures of coal seams [11, 12]. In the past decades, hydraulic fracturing technology has been widely applied to coal mine production in numerous countries, including China, USA, Canada, and Australia [13, 14].

Previous research has shown that traditional hydraulic fracturing technologies employ a constant higher water pressure than the rock strength to fracture the rock [15]. Thus, to realize an ideal fracturing effect, traditional hydraulic fracturing requires high flow, high pressure, and large amounts of water. Moreover, proppants and certain chemical agents are typically used to improve the effect of

hydraulic fracturing and maintain the stability of the fracture. These proppants and chemical reagents may enter the formation water and, consequently, pollute and damage the CBM reservoirs [16–18]. In addition, high-pressure equipment required to perform hydraulic fracturing in underground coal mines should have more complex sealing requirements, which significantly increases the safety risks. Utilization of the pulse hydraulic fracturing technology has been proposed to overcome this limitation [19]. Under a low impulsive load, more secondary cracks will be generated and the surface area of coal increases to promote gas desorption. At present, this technology has been the focus of research.

During pulse hydraulic fracturing, the persistent pulse waves propagate into coal rock, and the periodically alternating stresses generated under the peak pressure and base pressure are repeatedly applied to the coal mass. Eventually, due to the influence of cyclic loads at different frequencies, the fatigue failure of pores and cracks in coal gradually becomes more obvious, thus promoting the formation of new pores and cracks. Li et al. [20] investigated the mechanism of crack propagation during pulse hydraulic fracturing by utilizing the triaxial mechanical test system and acoustic emission. Similarly, Li et al. [21] carried out field testing at Yuwu Coal Mine (Shanxi Province, China) with pulse hydraulic fracturing. The S2107 coal seam was selected as the test coal seam, showing high gas content and coal and gas outburst hazard. The pulse hydraulic fracturing technology was used in the cross-measure boreholes from the high-level roadway to the driving roadway to improve the effect of gas drainage and ensure safety during the production. The test results revealed that the amount of gas extracted from the coal seams treated with pulse hydraulic fracturing separately increases by 3.32- and 3.07-fold relative to ordinary boreholes. Wang et al. [22] analyzed the influence of the pulse pressure on the formation and propagation of cracks in coal through numerical simulation. The results showed that the radius of influence of pulse hydraulic fracturing in coal seams reaches 8 m, and the total amount of the gas extraction rises by 3.6-fold; the flow of gas extraction reaches ≤50 L/min. However, the above studies did not thoroughly investigate the mechanism of pulsating hydraulic slitting at the microlevel.

As a special porous medium, natural coal mass exhibits many microporous characteristics, including porosity, pore size distribution, and pore volume [23–25]. The pore characteristics of coal are closely related to the adsorption capacity of gas in coal seams and also greatly influence the dynamic characteristics of gas [26–29]. The effect of cyclic loading may influence the characteristics of micropores in coal matrix in the process of improving permeability of coal seams through pulse hydraulic fracturing. Thus, cyclic loading affects the processes of gas migration, such as gas desorption, diffusion, and seepage in coal seams. Therefore, investigating the influence of cyclic loading on the characteristics of micropores in coal may provide an important theoretical basis for analyzing the microdynamic characteristics of gas during pulse hydraulic fracturing.

Based on the above evidence, seven groups of loading tests at different frequencies and amplitudes were performed on anthracite coal obtained from Shanxi Province, China, using a fatigue-testing machine. Afterwards, by applying a PoreMaster GT-60 Mercury-intrusion apparatus, the influence of the frequency and amplitude on the structural characteristics (e.g., mercury-injection and -ejection curves, pore size distribution, porosity, and specific surface area) of pores in coal samples was analyzed. Finally, the law and mechanism of action of the loading frequency and amplitude on pores in coal samples were comprehensively analyzed. The aim of this research study was to provide an important theoretical basis for the field application of pulse hydraulic fracturing technology in coal mines.

2. Materials and Methods

2.1. Preparation of Coal Samples. Anthracite coal obtained from Yangquan Mining Area in Shanxi Province, China, was used for the test. The location of Yangquan Mining Area is shown in Figure 1. The blocky coal samples were immediately sealed after collection from the fresh working face, packed, and sent to the laboratory.

The anisotropy of coal samples would influence the cyclic loading tests. Hence, the coal samples were crushed and processed into a briquette prior to testing and analysis for pores. The briquette is prepared mainly according to the following two steps: (1) (preparation of pulverized coal) the coal blocks were ground into fine powder particles by successively using a crusher and a grinder; afterwards, the powder particles were screened using standard sieves to attain particles of pulverized coal with pore size ranging 0.2–0.25 mm; and (2) (molding under compression) 200 g of pulverized coal and some water was loaded into a mold (diameter: 50 mm) and pressed for 20 min under the forming pressure of 100 MPa using a material testing machine with 200 t. Through this approach, coal samples were formed (the process required 10 min to load the pressure to the preset value at the loading rate of 20 kN/min).

2.2. Cyclic Loading Test. As shown in Table 1, seven groups of loading conditions were designed to investigate the influence of cyclic loading at different frequencies and amplitudes on the pore structure of anthracite coal.

During cyclic loading, a sample under loading for 20 min subjected to the forming pressure together with the mold was placed onto the fatigue-testing machine (Figure 2). According to the loading conditions in Table 1, the coal sample was loaded for 6 h, with sine waves as the loading waveform. After the loading was completed, the mold and sample were removed; furthermore, the mold was opened using a spanner to extract the final sample, whose length was measured with a Vernier caliper. Finally, after being subjected to loading, the coal particles with size ranging 1–3 mm were obtained from the sample using a knife, to be used as the test coal samples for the Mercury-intrusion test.

2.3. Determination of Pore Structure. The test was performed using the PoreMaster GT-60 Mercury-intrusion apparatus (Quantachrome Instruments, Boynton Beach, FL, USA) to

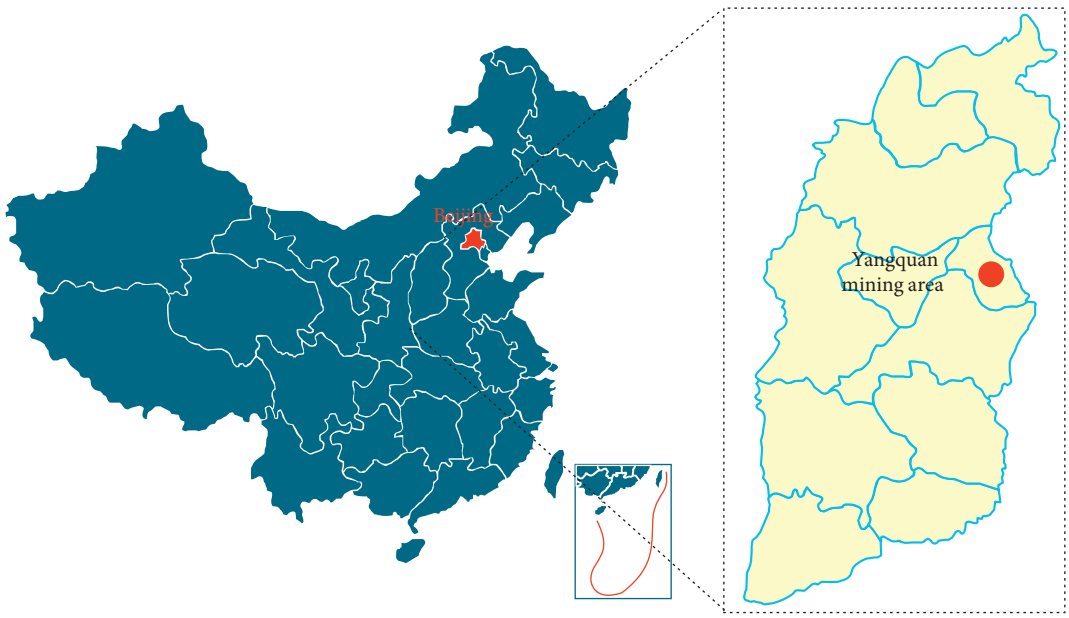

Figure 1: Location of Yangquan mining area.

Table 1: Loading conditions for the cyclic loading tests.

Group	Test condition		Loading time (h)
	Loading frequency (Hz)	Pressure amplitude during loading (MPa)	
1	10	12–18	
2	7		
3	4		6
4	7	10–20	
5		14–16	
6	—	15	
7	—	—	—

Note. In the test groups 1–5, only the frequency or amplitude was changed; in the control group 6, the frequency or amplitude was fixed; in the blank control group 7, cyclic fatigue loading was not performed.

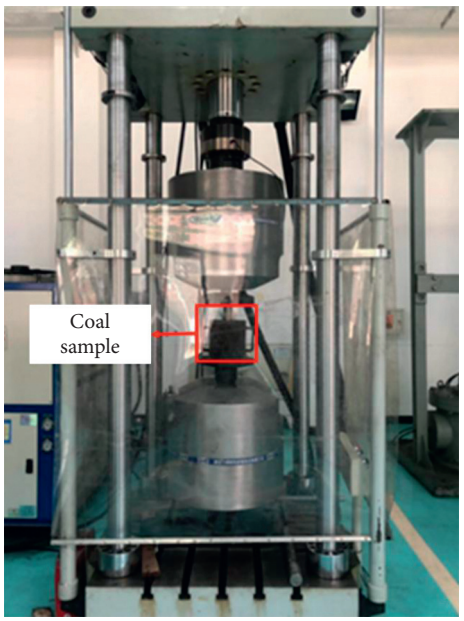

Figure 2: Fatigue-testing machine.

measure the volume of pores with diameter ranging 1,000–0.0035 μm (Figure 3). The apparatus is equipped with two low-pressure ports and two high-pressure ports. It is necessary to apply the low-pressure port and Mercury-injection station when measuring the volume of pores with size ranging 7–99 μm. The low-pressure examination port (under pressure of 0.2–50 psi) was used to inject Mercury with a sample tube, which measured the volume of pores with diameter ranging 1.0–4.3 μm. The high-pressure examination port (Figure 3) is utilized under pressure of 20–60,000 psi. The test data were processed using Washburn's equation [30] shown as follows:

$$p_c = \frac{2\sigma \cos \theta}{r}, \quad (1)$$

where p_c, σ, θ, and r refer to the additional pressure (MPa) of the applied liquid, surface tension (dyn/cm^2) of Mercury, wetting contact angle of Mercury, and radius (nm) of the pore throat, respectively.

Washburn's equation provides a simple relationship between the pressure and pore radius. Therefore, during the Mercury-intrusion test, it was feasible to attain the distribution of the pore radius by tracing the relationship between the amount of Mercury injected into pores and the constantly increasing pressure. Pores with different sizes show diverse degrees of resistance to Mercury; higher external pressures indicate smaller pore sizes in coal to which Mercury can enter [31]. Some other analysis parameters (e.g., specific surface area and porosity) can also be obtained by analyzing changes in the volumes of injected and ejected Mercury and pressures [32]. Of note, the pore distribution in coal samples under different loading conditions compared in this study was investigated the absence of any stress. Therefore, the influence of cyclic loading on pores can be determined to a certain extent through comparison before and after the stress-free condition.

3. Results and Discussion

3.1. Influence of Different Loading Frequencies on Pore Characteristics of Coal Mass. To investigate the influence of different loading frequencies on the pore characteristics of coal mass, tests were performed at loading frequencies of 4, 7, and 10 Hz and loading amplitude ranging 12–18 MPa (frequency magnitude that engineering applications can achieve). Moreover, the test results were compared with those attained in the control group under a steady pressure (15 MPa).

3.1.1. Mercury-Injection and Mercury-Ejection Curves. Figure 4 shows the mercury-injection and mercury-ejection curves of samples at different loading frequencies. The mercury-intrusion curves in the test groups at different loading frequencies and the control group presented a similar shape: a large growth amplitude in the low-pressure mercury-injection stage. Under the pressure of approximately 15 MPa, the curves became gentle, and they slowly rose with increasing pressure. In contrast, the mercury-

Figure 3: PoreMaster GT-60 Mercury-intrusion apparatus (Quantachrome Instruments).

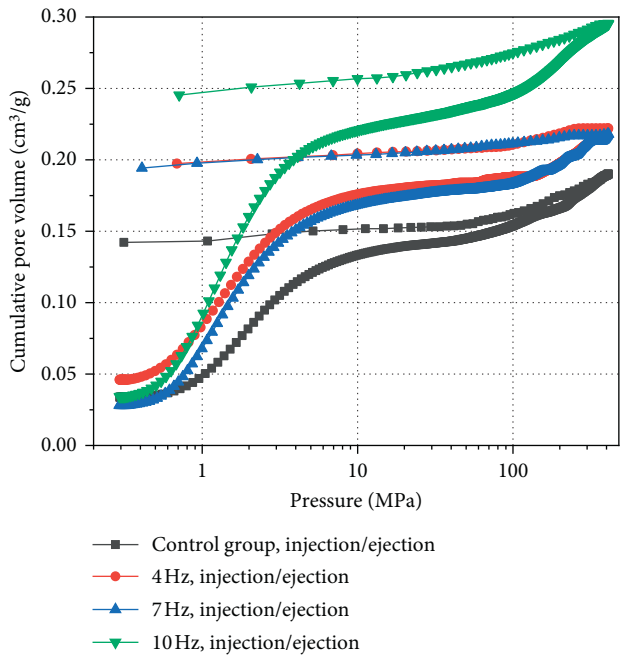

Figure 4: Mercury-intrusion curves of samples at different loading frequencies.

ejection curves started to separate from the injection ones under the initially high pressure, illustrating the hysteresis phenomenon. However, the final contents of Mercury injected are different, implying that the loading frequency influences the pore characteristics of coal samples to some extent. As shown in Figure 4, the highest final content of Mercury injected in the test group was shown at the loading frequency of 10 Hz, and the contents of Mercury injected in the test groups at 7 and 4 Hz differed only slightly. However, the contents of Mercury injected in the three test groups were significantly larger compared with those of the control group. It was also found that the mercury-injection and mercury-ejection curves in the two sample groups at the loading frequencies of 7 and 4 Hz were similar. This finding

indicates that, with the same amplitude, the pores in samples increase when loading sine waves with different frequencies are used. Moreover, the most remarkable influence was observed at the loading frequency of 10 Hz. In contrast, there was no great difference shown at low loading frequencies. Additionally, in terms of the difference in cumulative contents of the Mercury injected and ejected, the differences of the test groups at different loading frequencies were obviously larger than those of the control group. This result implies that when loading sine waves at different frequencies are used, the pores in samples favorably develop, and the proportion of seepage pores increases, thus optimizing the connectivity of pores.

3.1.2. Pore Size Distribution. Figure 5 shows the pore size distribution under four loading conditions, demonstrating a relatively similar overall shape to that of the control group. The pore size distribution was relatively concentrated, and the corresponding pore size ranges of two peaks were approximated; however, the peaks of the size range of the seepage pores in several test groups marginally shifted rightward; higher loading frequencies were associated with larger shift amplitudes. In other words, the peak pore volume slightly varied towards the range of macropores. The difference is that the global pore volume of the coal samples loaded with sine waves at different frequencies rose at different amplitudes, in which the pore volume of the test group at the loading frequency of 10 Hz showed the most significant growth amplitude, followed by the test groups at 7 and 4 Hz. In terms of the distribution of seepage pores and adsorption pores, the volumes of the former greatly increased, while those of the latter were similar.

3.1.3. Porosity and Percentage of Pore Volume. The division scheme of the pore size proposed by Hodot was employed in the test; pores were divided into macropores (>1,000 nm), mesopores (100–1,000 nm), transition pores (10–100 nm), and micropores (<10 nm) [33]. Micropores are space-storing gas; transition pores provide the space for gas diffusion; mesopores offer the space for slow gas flow; and macropores are space for strong flow of gas. Therefore, scholars also termed the pores with a size <100 nm (i.e., micropores and transition pores) adsorption pores, while mesopores and macropores with a size >100 nm are termed seepage pores [28, 34].

Table 2 displays the comparison data of the percentage of the pore volume and porosity under four loading conditions. In terms of the total porosity, the overall porosities of the samples loaded with sine waves at different frequencies increased slightly; higher loading frequencies were linked to higher total porosities. This indicates that the porosities of coal samples are markedly enhanced after performing cyclic loading with sine waves at different frequencies. Regarding the classification based on the pore size (Figure 6), the corresponding porosities contributed by pores of various size ranges also varied at different amplitudes. The porosities contributed by seepage pores delivered a large growth amplitude: it nearly doubled in the test group at 10 Hz, while

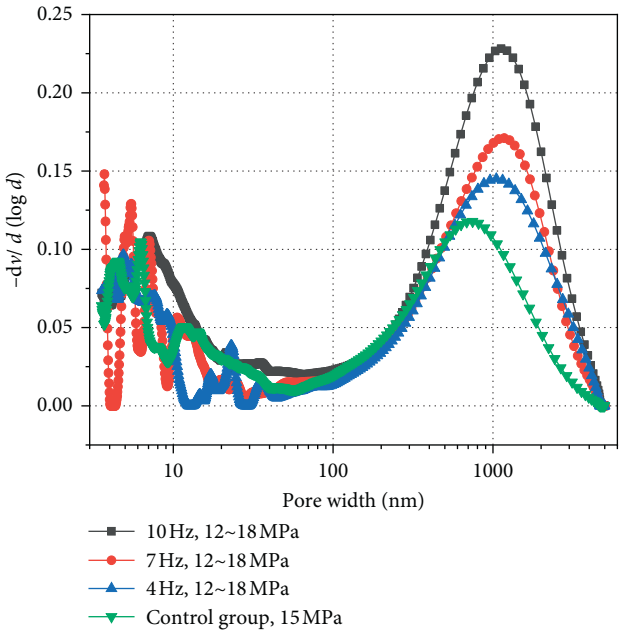

Figure 5: Density functions of pore volume distribution at different loading frequencies.

those in the test groups at 7 and 4 Hz increased by 3.41% and 2.04%, respectively. The porosities contributed by adsorption pores exhibited a nonsignificant increase: those in the test groups at 4 and 7 Hz hardly differed from those in the control group, and only the porosity contributed by adsorption pores in the test group at 10 Hz was slightly increased.

Table 3 shows the percentages of pore volume at different loading frequencies. The volume ratio of the adsorption pores to seepage pores in the control group was approximately 1 : 2. In contrast, the volume ratios of the adsorption pores to seepage pores in several test groups were approximately 1 : 3, and the proportion of the adsorption pores markedly decreased. This shows that loading sine waves with different frequencies can promote the expansion of pores and even fractures in coal samples. As a result, micropores and transition pores develop into mesopores and macropores, and new pores and fractures appear, thereby significantly improving the porosity of coal mass. However, the amplitude at which new pores and fractures initiate is lower than that at which pores expand. Thus, the porosity contributed by the adsorption pores nonsignificantly increases, while that contributed by seepage pores markedly rises.

3.1.4. Specific Surface Areas of Pores. The specific surface area of pores in coal mass is an important parameter for describing the pore characteristics. It is an important factor influencing the adsorption and desorption properties of gas in coal mass [5, 35, 36]. Figure 7 shows the distribution of the specific surface area of pores with the unit diameter under different loading frequencies, that is, the change in the relationship between the distribution density function $ds(d)$ for the specific surface area and the diameter d. The development trend of curves shown in Figure 8 illustrates that

Table 2: Percentages of the pore volume and porosities of coal mass at different loading frequencies.

Loading condition		Porosity (%)				
Frequency (Hz)	Amplitude (MPa)	Micropores (<10 nm)	Transition pores (10–100 nm)	Mesopores (100–1,000 nm)	Macropores (>1,000 nm)	Porosity (%)
4		2.42	0.69	2.06	7.55	12.71
7	12–18	2.02	1.42	5.15	5.83	14.41
10		3.15	2.11	5.88	8.68	19.81
—	15	2.15	1.60	4.40	3.18	11.32

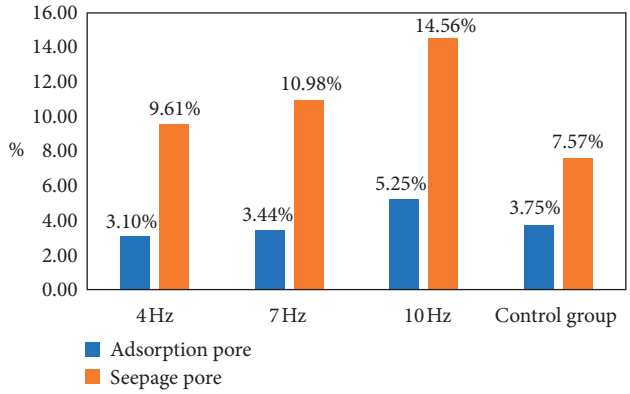

Figure 6: Distribution of the porosities contributed by adsorption and seepage pores at different loading frequencies.

Table 3: Percentages of the pore volume at different loading frequencies.

Loading condition		Percentage of the pore volume (%)					
Frequency (Hz)	Amplitude (MPa)	Micropores	Transition pores	Adsorption pores	Mesopores	Macropores	Seepage pores
4		18.31	5.41	23.72	41.57	34.72	76.28
7	12–18	14.00	9.27	23.27	39.88	36.85	76.73
10		14.91	11.76	26.67	37.20	36.13	73.33
—	15	16.70	17.15	33.85	47.66	18.49	66.15

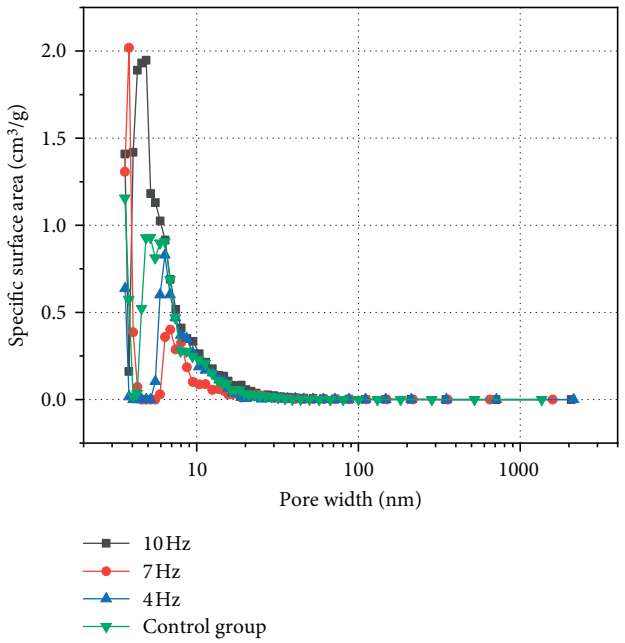

Figure 7: Distribution densities of the specific surface area of pores in coal mass at different loading frequencies.

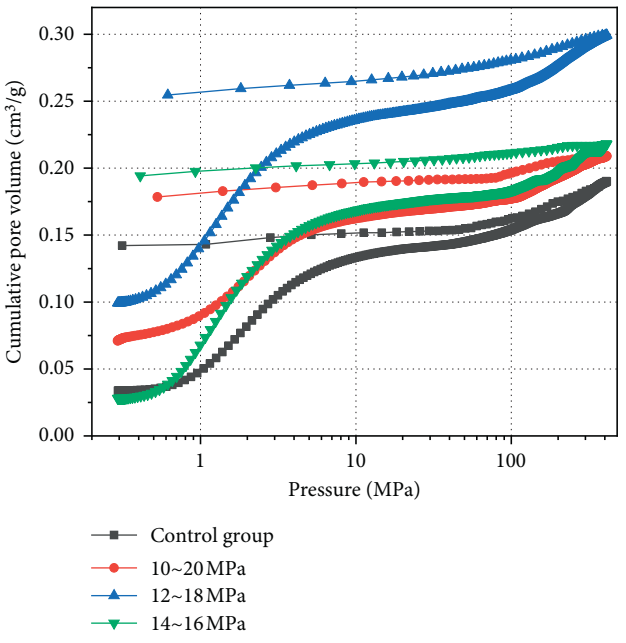

Figure 8: Mercury-intrusion curves of samples at different loading amplitudes.

the distribution densities of the specific surface area of all samples in the test were generally increased at first. Subsequently, they were reduced with the increasing pore size; they all reached the maximum before the pore size reached 10 nm. The peak in the test group at 10 Hz was observed at 4.57 nm, and the two peaks in the test group at 7 Hz separately appeared at 3.82 nm and 6.87 nm; the peak in the test group at 4 Hz was found at 6.37 nm, while that in the control group appeared at 6.36 nm. The growth of the distribution density shows that the growth rate of the cumulative specific surface area of pores in coal samples was gradually accelerated, and the specific surface area reached the peak at the peak of the distribution density. At the peak of the distribution density, the number of pores in coal samples with the corresponding size was the largest, or the length of pores was the largest, and the specific surface area was the largest. Based on this condition, the pores presented the strongest capacity of gas storage; in contrast, the capacity of pores for storing gas was gradually reduced.

Based on this evidence, the following conclusions can be drawn: the difference in loading frequencies influences the pore characteristics of coal samples to some extent; the pore volume generally increases significantly; although mesopores constitute the majority, followed by macropores, micropores, and transition pores, the proportions of mesopores and macropores increase, whereas those of micropores and transition pores slightly decline. This implies that the change in loading frequency exposes the coal mass to long-term fatigue loading. As a result, internal pores or fractures develop, and some micropores and transition pores are expanded and transformed into mesopores and macropores in the loading process; moreover, new pores and fractures are generated.

3.2. Influence of Different Loading Amplitudes on Pore Characteristics of Coal Mass. To investigate the influence of different loading amplitudes on the pore characteristics of coal mass, tests were carried out by separately selecting loading amplitudes (10–20, 12–18, and 14–16 MPa) and loading frequency (7 Hz). Furthermore, the results of the test were compared with those of the control group with a steady pressure (15 MPa) to analyze the influence law of the change of the loading amplitudes on the pore characteristics of coal samples.

3.2.1. Mercury-Injection and Mercury-Ejection Curves. Figure 8 shows the mercury-intrusion curves concerning the relationship between the cumulative content of Mercury injected in samples and mercury-injection and mercury-ejection pressures after loading sine waves at different amplitudes and frequency of 7 Hz. The curve in the control group under a steady pressure of 15 MPa was utilized as the reference curve. The shapes of mercury-intrusion curves in the four groups were similar. In the initial mercury-injection stage under low pressure, the mercury-injection curves abruptly rose and gently increased when the mercury-injection content reached two-thirds of the final overall content of Mercury injected. The curves slowly grew with the increasing pressure. The change in the mercury-ejection stage was similar to that observed in the mercury-intrusion curves at different loading frequencies in the last section: hysteresis was initiated in the initial mercury-ejection stage under high pressure. The generation of hysteresis is related to the existence of "ink bottle"-shaped holes in coal. Hysteresis is caused because the Mercury inlet pressure used to completely fill such holes with Mercury is different from the Mercury withdrawal pressure utilized to completely empty Mercury. However, the final contents of Mercury injected in the four test groups markedly differed. Relative to the test groups with different loading frequencies, the final contents of Mercury injected in the test groups loaded at different amplitudes demonstrated a smaller difference. The test group with the loading amplitude of 14–16 MPa showed the highest final content of Mercury injected (approximately 0.3 cm^3/g), followed by the test groups (approximately 0.2 cm^3/g) with the loading amplitudes of 12–18 and 10–20 MPa; among these two groups, the content of Mercury injected was higher in the test group with the loading amplitude of 12–18 MPa; the final content of Mercury injected was the lowest in the control group. However, the differences between the final content of Mercury injected in the test groups with the loading amplitude of 12–18 MPa and 10~20 MPa and the control group were nonsignificant. This indicates that when the loading frequency is unchanged, while the amplitude varies, the pores in coal samples are greatly affected; also, larger amplitudes are linked to lower final pore volumes, showing a negative correlation. The most remarkable influence was noted in the test group with the loading amplitude of 14–16 MPa. In terms of the difference between the cumulative contents of Mercury injected and ejected, the differences in the test groups loaded with different amplitudes were slightly larger than those observed in the control group. This indicates that changes in the loading amplitude of sine waves lead to the development of pores in coal samples and increase the seepage pores, thereby improving the connectivity of pores.

3.2.2. Pore Size Distribution. Figure 9 shows the distribution density functions of pore volumes under four loading conditions. The four curves with a similar shape presented two peaks. The pore size ranges corresponding to the peaks were relatively similar ($d < 10$ nm and $d = 1{,}000$ nm, respectively). However, the corresponding pore sizes of the peaks of seepage pores at 12–18 MPa and 14–16 MPa exhibited a nonsignificant rightward shift, in which the deviation value at 12–18 MPa was larger, implying that the peak pore volume slightly shifted to macropores. Moreover, the overall pore volumes of the two test groups were greatly larger than those of the control group. According to the distribution of seepage and adsorption pores, the pore volume of the former was more markedly increased, while that of the latter was less significantly increased. Nevertheless, the overall pore volume of the test group at the loading amplitude of 10–20 MPa decreased at a small amplitude relative to the control group. Among the several loading conditions, this was the only one under which the

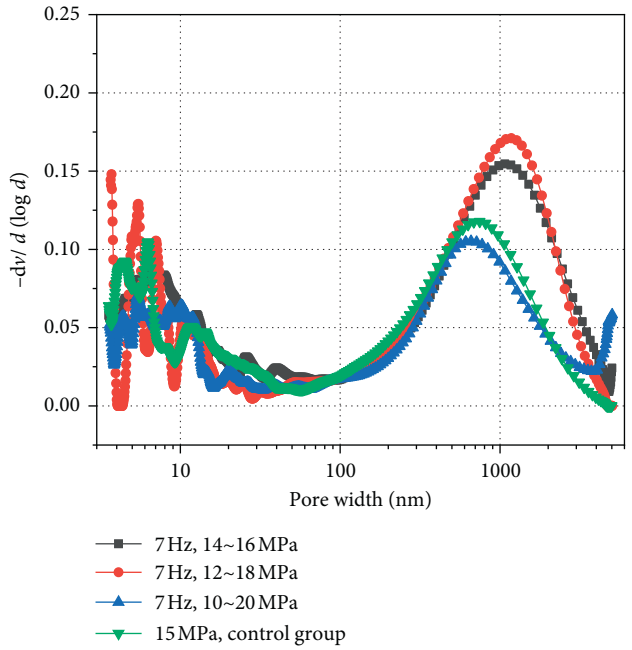

Figure 9: Distribution density functions of the pore volumes at different loading amplitudes.

peak distribution density of the pore volume was lower than that of the control group. This finding reveals that the loading condition of the test group possibly presents a small-amplitude inhibitory effect or nonsignificant promotive effect on the development of the pore volume of coal samples with different pore sizes.

3.2.3. Porosities and Percentages of the Pore Volume. Table 4 lists the comparison data of the percentages of the pore volumes and porosities under four loading conditions. The test groups at amplitudes of 14–16 and 12–18 MPa exhibited the highest total porosities, which were similar (14.47% and 14.41%, respectively). Relative to the porosity (11.32%) of the control group, the test group with the largest amplitude of 10–20 MPa only showed porosity of 10.22%, which was reduced by 1%. Regarding the porosity, the loading condition of 10–20 MPa showed an inhibitory effect on the development of pores, and the pores were slightly closed. The variations in the porosities contributed by adsorption and seepage pores also differed; the porosities contributed by seepage pores at 14–16 and 12–18 MPa were markedly increased by >10%. However, the porosity contributed by seepage pores in the test group at 10–20 MPa (only 6.92%) was lower than that of the control group, and the lowest among those of the test groups, as shown in Figure 10. Moreover, the porosity contributed by adsorption pores was slightly increased only in the test group at 14–16 MPa, while those in the test groups at 10–20 (3.30%) and 12–18 MPa (3.44%) were lower than those of the control group.

Table 5 shows that the volume ratios of the adsorption pores to seepage pores in the test groups and control group approximated 1 : 2; only the volume ratio of adsorption pores to seepage pores in the test group at 12–18 MPa approximated 1 : 3; the proportion of the adsorption pores was not markedly changed. These findings show that the change in the loading amplitude during the test exerted a non-uniform effect on promoting the formation of pores in coal samples. With the increase in loading amplitude, the seepage pores of coal showed an initially increasing trend followed by a decreasing trend, while the adsorption pores of coal showed a decreasing trend. Compared with the conventional control group (constant 15 MPa), the loading amplitude in the experimental group was the smallest (14–16 MPa), and the adsorption pores and seepage pores showed an increasing trend. The above experimental observations showed that the increase in loading amplitude can promote the expansion of existing pores or fractures, as well as the initiation of new pores and fractures. Although there was a difference in the degree of promotion of expansion and initiation, overall, the total pores in the coal sample were increased. When a loading amplitude of 10–20 MPa is used, the adsorption seepage pore porosity decreased. This showed that 10–20 MPa loading condition for the development of pore expansion inhibition and reaction, coal sample after extrusion force to change substantially, release, internal sample particles is compressed and intergranular pore, hole and the hole in the collapse of pore structure, transition into pores, holes, and microporous and transition hole by compaction, the compaction, the aperture range was lower than that of Mercury-injection experiment can measure range.

3.2.4. Specific Surface Area of Pores. Figure 11 shows the distribution of the specific surface area of pores with the unit diameter under different loading amplitudes. There is the relationship of change between the distribution density function $ds(d)$ of the specific surface area and the diameter d. According to the development trend noted in the curves, the distribution densities of the specific surface areas of all samples during the test were initially increased and subsequently decreased with the increase in pore size; they all reached the maximum before the pore size reached 10 nm. The peak in the test group at the loading amplitude of 10–20 MPa appeared at 5.18 nm, and the test group at 12–18 MPa presented two peaks at 3.82 nm and 6.87 nm; the peak in the test group at 14–16 MPa occurred at 4.31 nm, while that in the control group was found at 6.36 nm. The growth of the distribution density implies that the cumulative specific surface area of pores shows a gradually accelerated growth rate and reaches the peak at the peak of the distribution density. At the peak of the distribution density, the number of pores in samples with the corresponding size (mainly concentrated between 3.5 and 30.0 nm) was the largest, or the length of pores was the largest, and the specific surface area was the largest. Such pores demonstrated the strongest capacity for gas storage; in contrast, the capacity of pores for gas storage was gradually reduced.

According to the above evidence, the following conclusions can be drawn: the difference in the loading

Table 4: Percentages of the pore volume and porosities of coal mass at different loading amplitudes.

Loading condition		Porosity (%)				
Frequency (Hz)	Amplitude (MPa)	Micropores (<10 nm)	Transition pores	Mesopores	Macropores	Porosity (%)
	10–20	1.95	1.35	3.35	3.57	10.22
7	12–18	2.02	1.42	5.15	5.83	14.41
	14–16	2.51	1.77	4.97	5.22	14.47
—	15	2.15	1.60	4.40	3.18	11.32

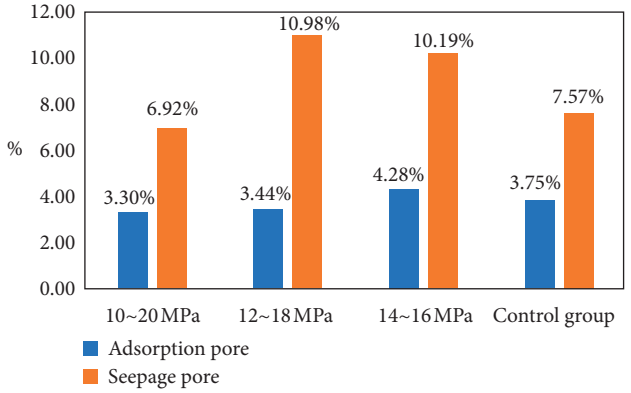

Figure 10: Distribution of porosities contributed by adsorption and seepage pores at different loading amplitudes.

Table 5: Percentages of the pore volume at different loading amplitudes.

Loading condition		Percentage of the pore volume (%)					
Frequency (Hz)	Amplitude (MPa)	Micropores (<10 nm)	Transition pores (10–100 nm)	Adsorption pores	Mesopores (100–1,000 nm)	Macropores (>1,000 nm)	Seepage pores
	10–20	17.51	15.23	32.74	46.10	21.16	67.26
7 Hz	12–18	14.00	9.27	23.27	39.88	36.85	76.73
	14–16	16.68	13.34	30.02	37.61	32.37	69.98
—	15	16.70	17.15	33.85	47.66	18.49	66.15

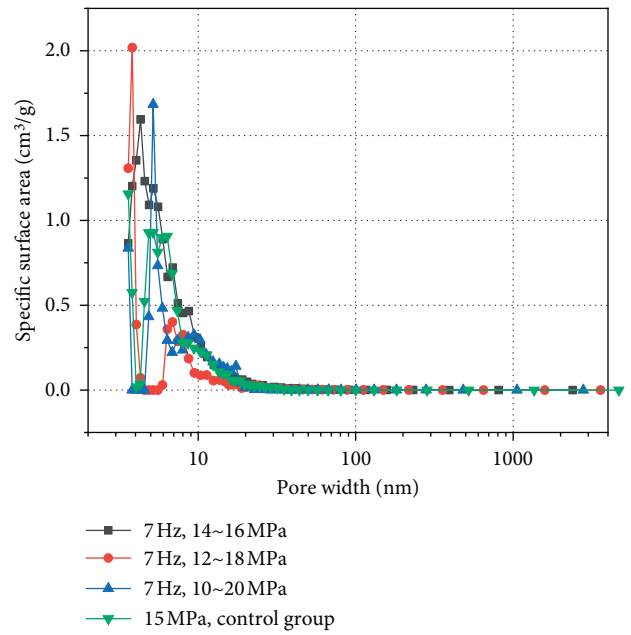

Figure 11: Distribution densities of the specific surface area of pores in coal mass at different loading amplitudes.

Table 6: Comparison of the growth amplitudes of the porosity under different loading conditions.

Frequency (Hz)	Amplitude (MPa)	Total porosity	Growth amplitude (%)	Growth amplitude of adsorption pores (%)	Growth amplitude of seepage pores (%)
—	15	11.32	—	—	—
	10–20	10.22	−9.75	−12.00	−8.58
7	12–18	14.41	27.29	−8.37	45.02
	14–16	14.47	27.79	14.10	34.63
4		12.71	12.26	−17.33	26.95
7	12–18	14.41	27.29	−8.27	45.05
10		19.81	74.99	40.00	92.34

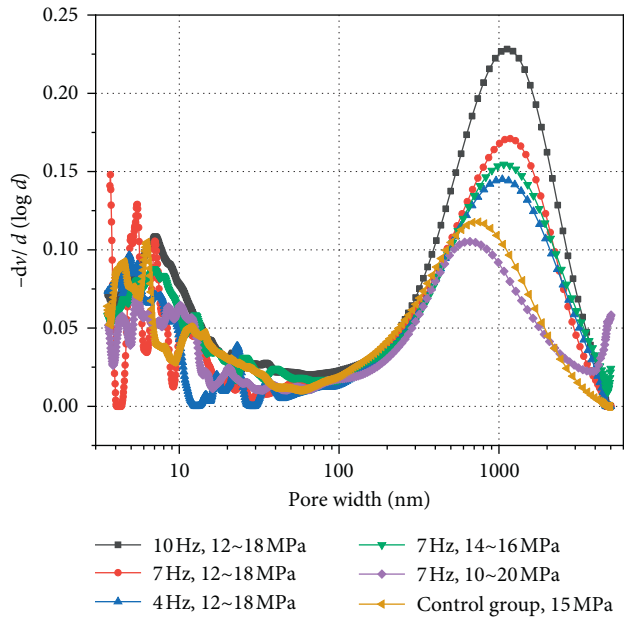

Figure 12: Distribution density functions of the pore volume under different loading conditions.

amplitudes influences the pore characteristics of coal sample; and the pore volume generally increases slightly. In terms of the classification based on the pore size, mesopores generally account for the majority, followed by macropores, micropores, and transition pores. Moreover, the change in loading amplitude promoted an initial increase followed by a decrease in the seepage pores of coal body, while the adsorption pores were gradually decreased. This implies that the change in amplitude plays a nonsignificant role in distinguishing the pores with different sizes. However, the porosity of the test group with the largest amplitude of 10–20 MPa decreased, and the corresponding peak of the pore volume slightly declined. These data reveal that a large loading amplitude exerts an opposite effect on the initiation and development of pores or fractures, which induces the collapse of macropores and mesopores. Furthermore, the pores were more compacted, thus leading to reduction of the porosity to lower levels than the original coal porosity or fracture occurrence degree.

4. Implications for Frequency and Amplitude Selection during Pulse Hydraulic Fracturing

According to the analysis described in Sections 3.1 and 3.2, the change in the loading frequency or loading amplitude influences the pore characteristics of coal samples. The influence was basically positive, promoting the initiation and development of pores; however, there was also negative influence noted.

Table 6 compares the effects of the change in amplitude and frequency on the porosity. Relative to the control group loaded under a steady pressure, the growth amplitude of the porosity ranged from −9.7450% to 27.7895% when changing the amplitude; lower amplitudes were linked to larger growth amplitudes. The growth amplitude of the total porosity varied between 12.2637% and 74.9861% when changing the frequency; higher frequencies were associated with larger growth amplitudes. Regarding the total porosity, the change in frequency imposed obviously greater influences than the change in amplitude.

In terms of seepage and adsorption pores, the growth amplitude of the porosity of the seepage pores in the test group with changing frequency ranged from −8.58% to 45.02%, while that of adsorption pores was between −8.37% and 14.10%; the porosity contributed by seepage pores in the test group with changing amplitude presented a growth amplitude of 26.95–92.34%, while that contributed by adsorption pores delivered a growth amplitude between −17.33% and 40.00%. This indicates that the loading frequency exerts a greater negative influence on adsorption pores; correspondingly, it exhibits a greater positive influence on seepage pores. The effects of the loading amplitude on the growth amplitudes of the porosity contributed by the two types of pores were nearly equivalent.

By comparing the distribution density functions of the pore volume under different loading conditions (Figure 12), it was found that the function curve of the pore volume in the test group at 10 Hz and 12–18 MPa was located markedly above those of the other test groups. Moreover, only the function curve of the pore volume in the test group at 7 Hz and 10–20 MPa was situated below that of the control group. The curves of the three groups at different loading amplitudes were denser than those at different loading frequencies, implying that the change in amplitude marginally

influences the pore volume, whereas the change in frequency greatly changes the pore volume of samples.

The final purpose of pulse hydraulic fracturing in underground coal mines is to increase the permeability of coal seams and further improve the amount of gas extraction. The results of this research show that the seepage pores in coal samples rose significantly in response to increasing frequency. This indicates that, in field construction, the fracturing effect can be strengthened by enhancing the frequency. However, enhancement of the frequency is associated with an increase in construction cost. Further research on this topic is warranted for the selection of the proper frequency and evaluation of the economic cost. Additionally, the results described in Section 3.2 show that the largest increment of seepage pores is observed at the amplitude of 12–18 MPa. Thus, during field construction, it is suggested to perform pulse hydraulic fracturing by selecting the amplitude within this range.

5. Conclusions

Based on the findings of the present study, the following conclusions can be drawn.

Firstly, by maintaining the loading amplitude of sine waves unchanged while changing their loading frequency, the overall porosity and the pore volume increase at different amplitudes. The increase in loading frequency exerts a more significant promotive effect on the initiation and development of pores and fractures and drives the transformation of micropores and transition pores into mesopores and macropores. The proportion of the seepage pores grows, and the change in the loading amplitude of sine waves delivers a complex influence on the pore characteristics of anthracite coal.

Secondly, when the frequency of the loaded sinusoidal wave is unchanged, the amplitude of the loaded sinusoidal wave is altered to promote change in coal seepage pores through an initial increase followed by a decrease, while the change in coal adsorption pores gradually decreases. When the loading amplitude increases, it influences the development and initiation of pores or fractures. This leads to the collapse of macropores and mesopores, and the pores become more compact.

Finally, the change in loading frequency has a greater impact on the pore characteristics of the briquette and a greater negative impact on adsorption pores than seepage pores. Amplitude of the change of adsorption and filtration could inhibit the growth of two types of pores, which is relatively close, active application in practice of changing load change coal pore properties, and if unable to meet the change of frequency and amplitude, at the same time, give priority to increasing frequency of choice to promote the initiation and development of pore, to be connected hole, and guide the internal pore gas form seepage.

Data Availability

All data, models, and code generated or used during the study are included in the manuscript.

Conflicts of Interest

The authors declare that they have no conflicts of interest to this work.

Acknowledgments

This work was supported by the National Natural Science Foundation of China (grant numbers 51674016 and 52074120), and the Fundamental Research Funds for the Central Universities (3142019005).

References

[1] Q. Zou, H. Liu, Y. Zhang, Q. Li, J. Fu, and Q. Hu, "Rationality evaluation of production deployment of outburst-prone coal mines: a case study of Nantong coal mine in Chongqing, China," *Safety Science*, vol. 122, Article ID 104515, 2020.

[2] H. Wang, B. Tan, Z. Shao, Y. Guo, Z. Zhang, and C. Xu, "Influence of different content of FeS2 on spontaneous combustion characteristics of coal," *Fuel*, vol. 288, Article ID 119582, 2021.

[3] A. Busch and Y. Gensterblum, "CBM and CO_2-ECBM related sorption processes in coal: a review," *International Journal of Coal Geology*, vol. 87, no. 2, pp. 49–71, 2011.

[4] E. Su, Y. Liang, Q. Zou, F. Niu, and L. Li, "Analysis of effects of CO_2 injection on coalbed permeability: implications for coal seam CO_2 sequestration," *Energy & Fuels*, vol. 33, no. 7, pp. 6606–6615, 2019.

[5] E. Su, Y. Liang, Q. Zou, M. Xu, and A. P. Sasmito, "Numerical analysis of permeability rebound and recovery during coalbed methane extraction: implications for CO_2 injection methods," *Process Safety and Environmental Protection*, vol. 149, pp. 93–104, 2021.

[6] H. Wang, X. Fang, F. Du et al., "Three-dimensional distribution and oxidation degree analysis of coal gangue dump fire area: a case study," *Science of The Total Environment*, vol. 772, Article ID 145606, 2021.

[7] Q. Zou and B. Lin, "Fluid-solid coupling characteristics of gas-bearing coal subjected to hydraulic slotting: an experimental investigation," *Energy & Fuels*, vol. 32, no. 2, pp. 1047–1060, 2018.

[8] F. Du and K. Wang, "Unstable failure of gas-bearing coal-rock combination bodies: insights from physical experiments and numerical simulations," *Process Safety and Environmental Protection*, vol. 129, pp. 264–279, 2019.

[9] A. Abdollahipour, M. Fatehi Marji, A. Yarahmadi Bafghi, and J. Gholamnejad, "DEM simulation of confining pressure effects on crack opening displacement in hydraulic fracturing," *International Journal of Mining Science and Technology*, vol. 26, no. 4, pp. 557–561, 2016.

[10] Q. Zou, H. Liu, Z. Cheng, T. Zhang, and B. Lin, "Effect of slot inclination angle and borehole-slot ratio on mechanical property of pre-cracked coal: implications for ECBM recovery using hydraulic slotting," *Natural Resources Research*, vol. 29, no. 3, pp. 1705–1729, 2020.

[11] Y. M. Lekontsev and P. V. Sazhin, "Directional hydraulic fracturing in difficult caving roof control and coal degassing," *Journal of Mining Science*, vol. 50, no. 5, pp. 914–917, 2014.

[12] Q. Zou, B. Lin, C. Zheng et al., "Novel integrated techniques of drilling-slotting-separation-sealing for enhanced coal bed methane recovery in underground coal mines," *Journal of Natural Gas Science and Engineering*, vol. 26, pp. 960–973, 2015.

[13] K. H. S. M. Sampath, M. S. A. Perera, P. G. Ranjith et al., "CH_4 CO_2 gas exchange and supercritical CO_2 based hydraulic fracturing as CBM production-accelerating techniques: a review," *Journal of CO_2 Utilization*, vol. 22, pp. 212–230, 2017.

[14] Y. Liu, X. Wen, M. Jiang et al., "Impact of pulsation frequency and pressure amplitude on the evolution of coal pore structures during gas fracturing," *Fuel*, vol. 268, Article ID 117324, 2020.

[15] X. Jingna, X. Jun, N. Guanhua, S. Rahman, S. Qian, and W. Hui, "Effects of pulse wave on the variation of coal pore structure in pulsating hydraulic fracturing process of coal seam," *Fuel*, vol. 264, Article ID 116906, 2020.

[16] J. Blunschi, J. Wang, and T. Ertekin, "Hydraulic fracturing mechanisms in coal: a review," *International Journal of Oil, Gas and Coal Technology*, vol. 14, no. 3, pp. 247–263, 2017.

[17] J. Zhou, S. Tian, L. Zhou et al., "Experimental investigation on the influence of sub- and super-critical CO_2 saturation time on the permeability of fractured shale," *Energy*, vol. 191, Article ID 116574, 2020.

[18] J. Chen, X. Li, H. Cao, and L. Huang, "Experimental investigation of the influence of pulsating hydraulic fracturing on pre-existing fractures propagation in coal," *Journal of Petroleum Science and Engineering*, vol. 189, Article ID 107040, 2020.

[19] Q. Li, B. Lin, and C. Zhai, "The effect of pulse frequency on the fracture extension during hydraulic fracturing," *Journal of Natural Gas Science and Engineering*, vol. 21, pp. 296–303, 2014.

[20] Q. Li, B. Lin, C. Zhai et al., "Variable frequency of pulse hydraulic fracturing for improving permeability in coal seam," *International Journal of Mining Science and Technology*, vol. 23, no. 6, pp. 847–853, 2013.

[21] Q. Li, B. Lin, and C. Zhai, "A new technique for preventing and controlling coal and gas outburst hazard with pulse hydraulic fracturing: a case study in Yuwu Coal Mine, China," *Natural Hazards*, vol. 75, no. 3, pp. 2931–2946, 2015.

[22] W. Wang, X. Li, B. Lin, and C. Zhai, "Pulsating hydraulic fracturing technology in low permeability coal seams," *International Journal of Mining Science and Technology*, vol. 25, no. 4, pp. 681–685, 2015.

[23] K. Jin, Y. Cheng, Q. Liu et al., "Experimental investigation of pore structure damage in pulverized coal: implications for methane adsorption and diffusion characteristics," *Energy & Fuels*, vol. 30, no. 12, pp. 10383–10395, 2016.

[24] F. Wang, Y. Cheng, S. Lu, K. Jin, and W. Zhao, "Influence of coalification on the pore characteristics of middle-high rank coal," *Energy & Fuels*, vol. 28, no. 9, pp. 5729–5736, 2014.

[25] B. Nie, X. Liu, L. Yang, J. Meng, and X. Li, "Pore structure characterization of different rank coals using gas adsorption and scanning electron microscopy," *Fuel*, vol. 158, pp. 908–917, 2015.

[26] E. Su, Y. Liang, X. Chang, Q. Zou, M. Xu, and A. P. Sasmito, "Effects of cyclic saturation of supercritical CO_2 on the pore structures and mechanical properties of bituminous coal: an experimental study," *Journal of CO_2 Utilization*, vol. 40, Article ID 101208, 2020.

[27] E. P. Barrett, L. G. Joyner, and P. P. Halenda, "The determination of pore volume and area distributions in porous substances. I. computations from nitrogen isotherms," *Journal of the American Chemical Society*, vol. 73, no. 1, pp. 373–380, 1951.

[28] Y. Cai, D. Liu, Z. Pan, Y. Yao, J. Li, and Y. Qiu, "Pore structure and its impact on CH4 adsorption capacity and flow capability of bituminous and subbituminous coals from Northeast China," *Fuel*, vol. 103, pp. 258–268, 2013.

[29] E. Su, Y. Liang, and Q. Zou, "Structures and fractal characteristics of pores in long-flame coal after cyclical supercritical CO_2 treatment," *Fuel*, vol. 286, p. 119305, 2021.

[30] E. W. Washburn, "The dynamics of capillary flow," *Physical Review*, vol. 17, no. 3, pp. 273–283, 1921.

[31] K. Zhang, Y. Cheng, K. Jin et al., "Effects of supercritical CO_2 fluids on pore morphology of coal: implications for CO_2 geological sequestration," *Energy & Fuels*, vol. 31, no. 5, pp. 4731–4741, 2017.

[32] H. Jiang, Y. Cheng, and L. Yuan, "A Langmuir-like desorption model for reflecting the inhomogeneous pore structure of coal and its experimental verification," *RSC Advances*, vol. 5, no. 4, pp. 2434–2440, 2014.

[33] B. B. Hodot, *Outburst of Coal and Coalbed Gas*, China Industry Press, Beijing, China, 1966.

[34] E. Su, Y. Liang, L. Li, Q. Zou, and F. Niu, "Laboratory study on changes in the pore structures and gas desorption properties of intact and tectonic coals after supercritical CO_2 treatment: implications for coalbed methane recovery," *Energies*, vol. 11, no. 12, p. 3419, 2018.

[35] X. Wang, D. Zhang, E. Su et al., "Pore structure and diffusion characteristics of intact and tectonic coals: implications for selection of CO_2 geological sequestration site," *Journal of Natural Gas Science and Engineering*, vol. 81, Article ID 103388, 2020.

[36] J. Pan, Y. Zhao, Q. Hou, and Y. Jin, "Nanoscale pores in coal related to coal rank and deformation structures," *Transport in Porous Media*, vol. 107, no. 2, pp. 543–554, 2015.